International Journal of Applied Earth Observations and Geoinformation 101 (2021) 102355

Contents lists available at ScienceDirect

International Journal of Applied Earth Observations and Geoinformation

journal homepage: www.elsevier.com/locate/jag

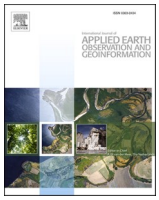

Biomass estimation of pasture plots with multitemporal UAV-based photogrammetric surveys

Izar Sinde-González [a,b,*], Mariluz Gil-Docampo [a], Marcos Arza-García [a], José Grefa-Sánchez [c], Diana Yánez-Simba [c], Patricio Pérez-Guerrero [d], Víctor Abril-Porras [d]

[a] Agroforestry Engineering Department, University of Santiago de Compostela, Higher Polytechnic School of Engineering, Campus Universitario s/n, 27002 Lugo, Spain
[b] Grupo de investigación Geoespacial, Departamento de Ciencias de la Tierra y la Construcción, Universidad de las Fuerzas Armadas ESPE, 171103, Av. General Rumiñahui s/n, Sangolquí, Ecuador
[c] Carrera de Ingeniería Geográfica y del Medio Ambiente, Universidad de las Fuerzas Armadas ESPE, Av. General Rumiñahui, s/n, 171103 Sangolquí, Ecuador
[d] Departamento de Ciencias de la Vida y la Agricultura, Carrera de Ingeniería Agropecuaria IASA I, Universidad de las Fuerzas Armadas ESPE, Sangolquí, Ecuador

ARTICLE INFO

Keywords:
Cultivated pastures
CSM
Precision agriculture
DTM
Aboveground biomass

ABSTRACT

Pastures account for more than 56% of the total agricultural area of Ecuador and constitute the main food source for livestock. Hence, the agile, affordable, and reliable quantification of aboveground biomass (AGB) is an essential task in grazing utilization and management. In this paper, a method to estimate the AGB via aerial photogrammetry with a low-cost UAV multirotor is proposed. Digital terrain models and crop surface models were generated from data captured during two flights at different times, and the volume between them was calculated. An empirical relationship between volume and dry biomass was obtained by harvesting and weighing some samples and deriving a density factor (DF). The method was tested over 54 plots with different types of forage under differential fertilization treatments. Fertilized annual ryegrass exhibited the best growth and highest biomass (2632 kg/ha). The estimation and calculation of the crop volume via UAV-based photogrammetry saves time and generates notably precise ($R^2 = 0.78$) information on the dry biomass.

1. Introduction

The main and most economical source of food for livestock in the Republic of Ecuador is grass. According to the National Institute of Statistics and Census (INEC), planted and natural pastures represented approximately 38.85% and 17.92%, respectively, of the total agricultural working area of 5,110,549 ha in 2019. In addition, grazing achieves the best yields among livestock feed systems (Grijalva et al., 1995). However, agricultural treatments such as fertilizers or soil amendments are not commonly used for this type of crop; thus, the achieved yields at the production level are not usually maximized. Increased knowledge about the dynamics of the biomass and net primary productivity of grasslands will facilitate better planning and use of resources.

1.1. Aboveground biomass estimation methods

Until recently, most of the existing methods for aboveground biomass (AGB) estimation at a local-scale level were based on destructive sampling (Catchpole and Wheeler, 2010) or simple visual assessment (Waite, 1994). However, with the advancement in sensor technologies and new platforms to mount these sensors, methods based on remote sensing (RS) are gaining considerable popularity. Some examples are studies based on ground-level instruments, which can reach high levels of confidence in the AGB estimation in some cases. For example, Busemeyer et al. (2013) used a tractor-pulling multi-sensor approach with 3D time-of-flight cameras, laser distance sensors and hyperspectral cameras, which reached an R^2 of 0.97 for triticale crops. However, in general, ground-based RS methods can only be used in certain parts of the study area, and discrete measurement and interpolation techniques are often required (Cevallos et al., 2018).

The low performance and generally high cost of terrestrial methods make unmanned aerial vehicles (UAVs) a very popular alternative for this purpose (Acorsi et al., 2019; Niu et al., 2019; Michez et al., 2020). UAV-based RS techniques can provide continuous spatial data, great performance for large areas and more flexibility in data acquisition with a certain degree of independence of weather conditions; thus, they found an ideal niche of application in estimating biomass (Bareth and Schellberg, 2018).

* Corresponding author.
E-mail address: izar.sinde@rai.usc.es (I. Sinde-González).

https://doi.org/10.1016/j.jag.2021.102355
Received 12 January 2021; Received in revised form 23 April 2021; Accepted 26 April 2021
Available online 6 May 2021

UAV-based multispectral and hyperspectral data can replace traditional techniques, as demonstrated in several studies. Visible near-infrared (VNIR) and short-wave infrared (SWIR) have brought a new perspective to this topic (Jenal et al., 2020; Hart et al., 2020). By building regression models between field measurements and vegetation indices (e.g., NDVI and enhanced vegetation index (EVI)), such imagery has been largely used in grassland AGB quantification (Stroppiana et al., 2015; Selsam et al., 2017). Deep learning algorithms are also finding an important application in the analysis of those multi-spectral data (Castro et al., 2020; Viljanen et al., 2018; Näsi et al., 2018; Grüner et al., 2020), driving a better construction of the models and improving the interpretation of results in AGB estimation.

Even at a high cost, light detection and ranging (LiDAR) was until recently considered the most reliable alternative to undertake surveys on plant masses. Due to the ability of this technique to penetrate dense vegetation, it can provide useful information regarding both horizontal and vertical structural information of plants obtain precise parameter retrieval. LiDAR approaches, terrestrial laser scanning (TLS) (e.g., Tilly et al., 2014) and airborne/UAV-based LiDAR (e.g., Eitel et al., 2014) have been widely used in vegetation analysis. Certainly, LiDAR is considered a reference technique for application in higher agricultural crops such as maize or in woody biomass estimation (i.e., forests or woody crops such as fruit trees, vineyards, olive groves, etc.). However, some previous research concluded that its use posed certain limitations in thinner vegetation layers such as grassland systems (Cooper et al., 2017).

1.2. UAV-based SfM photogrammetry approach

In the last decade, we have witnessed the fusion of conventional digital photogrammetry with computer vision algorithms (scale invariant feature transform (SIFT, (Lowe, 2004)), SfM (Westoby et al., 2012), multi-view stereopsis (MVS, (Furukawa and Accurate, 2007)), etc., which have greatly improved matching processes and made image set requirements more flexible. As a result of this merge, a new and more affordable image-based approach has arisen, which is often generalized as "SfM (structure-from-motion) photogrammetry". The main advantage of SfM photogrammetry over conventional digital photogrammetry is that it can deliver photogrammetric models from RGB images without requiring rigorous homogeneity in their levels of overlap, camera poses and calibrations (Fonstad et al., 2013). In contrast to the conventional workflow of photogrammetry, the SfM pipeline can simultaneously solve the camera pose and scene geometry. It is possible to use a highly redundant bundle adjustment based on feature matching in multiple overlapping images (Westoby et al., 2012). Afterwards, dense image matching is performed with a dense MVS algorithm, which computes a dense point cloud from the oriented images to obtain a 3D geometry. The main advantage of this type of processing is its ability to obtain results with photorealistic quality, good positional accuracy and a high degree of automation (Frankl et al., 2015; Micheletti et al., 2015).

The use of an image-based modelling process with SfM algorithms has been particularly widespread in classical topics for photogrammetry, such as cultural heritage (Arza-García et al., 2019; Pepe and Constantino, 2020) or mining (Pepe et al., 2020; Gul, 2019). Its use is also increasingly common in fields such as forestry (Iglhaut et al., 2019; Kachamba et al., 2016) and agriculture (Dash et al., 2017), where the previous approach had some difficulties (e.g., poor image correlation in vegetation layers). As mentioned above, the SfM photogrammetry workflow can ultimately yield 3D dense point clouds, similar to those produced by LiDAR, from which other products can be derived. For example, when applied to aerial images of a crop field, digital terrain models (DTMs) and crop surface models (CSMs) can be obtained and utilized to calculate the canopy heights and volumes (Belton et al., 2019; Calou et al., 2019; d'Oleire-Oltmanns et al., 2012).

Aerial photogrammetric techniques have been used for vegetation data gathering to improve the characterization and management of areas of ecosystems with high research interest (Cucho-Padin et al., 2019; Meneses et al., 2015; Mukherjee et al., 2019). This approach has also enabled the characterization of areas of dense vegetation and crop fields for efficient data management, which improves the processes for the conservation and development of these areas (Acevo-Herrera et al., 2010; Astapov et al., 2019; Guo et al., 2012; Maresma et al., 2016; Nawaz et al., 2019). Some studies with UAV-based photogrammetry have been performed to investigate issues such as drought (Torres-Sánchez et al., 2015).

Among different research topics in precision agriculture supported by UAV-based SfM photogrammetry, estimating AGB is probably one of the most explored issues, since it is directly related the net primary productivity. Examples include studies on cereal crops such as barley (Bendig et al., 2014), black oat (Acorsi et al., 2019), maize, (Zhu et al., 2019), and onion (Ballesteros et al., 2018). Although these studies obtained continuous and complete data at the plot level, none of the proposed methods could completely eliminate the typical destructive field sampling of traditional systematic sampling.

A small number of studies also specifically attempted to estimate the biomass in pastures with photogrammetry (e.g., Batistoti et al., 2019; Grüner et al., 2019; Lussem et al., 2020; Michez et al., 2019) using the correlation between the crop height obtained with the DTM and CSM and the biomass field samples. Most results showed that the crop height was a robust estimator for AGB, and the high spatial resolution in DTM-CSM datasets helped to improve the AGB estimation (Zhu et al., 2019). Gil-Docampo et al. (2020) proposed the use of the density factor (DF) as a simplified method to link field data with the volume information between DTM and CSM. This method relates the weight of the field sample to the volume of vegetation at each sampling point; thus, it provides an empirical relation between crop volumes and AGB. Although this can be a valid approach, research has been performed using a pre-existing LiDAR DTM (public source) of much coarser resolution (1 $m \cdot pix^{-1}$) than the CSM generated from UAV imagery (i.e., 0.02–0.05 $m \cdot pix^{-1}$). Some authors partially solved this problem using manually collected GPS points in the field to obtain the DTM (Batistoti et al., 2019), although this process is too labour-intensive for large areas of pasture. Lacking a DTM representing bare ground, another commonly adopted solution is to perform point cloud classification to separate ground points (DTMs) and crop surface points (CSMs) from the same dataset of images (Näsi et al., 2018). Although this process can be done with a single UAV flight, obtaining sufficiently many ground points from SfM output data is only feasible with sparse and discontinuous layers of vegetation, which is not usually the case for grasslands.

The present study aims to investigate the use of multitemporal UAV-based imagery and SfM photogrammetry to estimate the AGB of pastures at a fine spatial scale. The study tests the DF proposed by Gil-Docampo et al. (2020) and analyses challenging conditions caused by the small height of the forage crops. A methodology based on the indirect determination of the vegetation volume is applied to determine whether the total AGB of a small cultivar (i.e., pasture grass) can be estimated based on the SfM-derived CSM and DTM. To develop an easily reproducible and accessible solution for anyone interested in pasture management, we select a low-cost consumer-grade UAV to validate the methodology. We attempt to demonstrate whether the proposed method achieves acceptable accuracy in estimating the AGB from few field samples over three predominant forage types: *Lolium perenne*, *Lolium multiflorum* and *Pennisetum clandestinum*. Different crop treatments that allow greater efficiency in the use of resources for optimized production are identified in parallel.

2. Materials and methods

2.1. Study area and equipment

The study area is located on the El Prado IASA I farm in Sangolquí, which is in the province of Pichincha (Ecuador), and it belongs to the

Department of Life and Agricultural Sciences of the University of the Armed Forces (ESPE), as shown in Fig. 1. The study area covered 8210 m^2, and the arable area was 4320 m^2, which excluded the paths between plots. For the subsequent analysis of the crops, experimental units were implemented by dividing the area into 11 plots, each of which had an average area of 750 m^2. Each plot was divided into subplots with an average area of 80 m^2 and a 1 m distance between them. In total, 72 subplots were established in the study area, of which 54 were used for the study due to the presence of forest species with an approximate height of 40 m, since the shade from the trees prevented us from obtaining aerial photographs of the plots in the eastern part of the farm.

A commercial UAV DJI (Shenzen, China) Phantom 4 (i.e., a relatively low-cost apparatus) was used for imaging. With an average weight of 1.3 kg, this model can reach a speed of 72 km/h and resist wind speeds up to 10 m/s. The RGB built-in camera of the UAV had a 1/2.3-inch with a complementary metal oxide semiconductor (CMOS) sensor and a resolution of 12.4 megapixels.

To ensure adequate georeferencing, in terms of both planimetry and altimetry, ground control points (GCPs) were first established with 20-cm-diameter cylindrical cement cores. In total, 8 GCPs were distributed in the study area, as shown in Fig. 2. High-precision coordinates of the points were obtained using the static tracking method with a Trimble R8 (Sunnyvale, CA, US) GPS receiver (H: 3 mm + 0.1 ppm/V: 3.5 mm + 0.4 ppm), and the observation time for each point was approximately one and a half hours.

The EPEC station of the continuous monitoring infrastructure of Ecuador (REGME) was used as a baseline to reference the measurements, and the SIRGAS ECUADOR reference framework was established. The points were tracked on September 7, 2017 for GPS weeks 1963 and 237. Post-processing was performed with Trimble Business Center software.

For the digital photogrammetric processing of images, the Automatic Image Correlation (AIC) software Agisoft (Saint Petersburg, Russia) PhotoScan was used to generate spatial data and 3D models from a collection of disoriented images.

2.2. Flow chart of the process

The methodological flow of this study is shown in Fig. 3.

2.3. Plotting and fertilization

The experiment employed a factorial design with three variables: slope variation (3), type of fodder (3) and fertilization (2). Each experiment was repeated three times, and 54 experimental plots were evaluated in total.

Previous information for the study area obtained by the National Institute of Agricultural Research of Ecuador (INIAP) in 2017 was used to identify the initial differences in the nutrients in the soil (Ca, Fe and P). Fertilization was performed to address the detected phosphorus deficiencies in the previous analyses. The fertilizer (the % of guaranteed content of the compound was 10–30-10 of N-P-K, respectively) was timely applied according to the nutritional needs in a certain number of plots, and other experimental areas were unfertilized (Fig. 4). This type

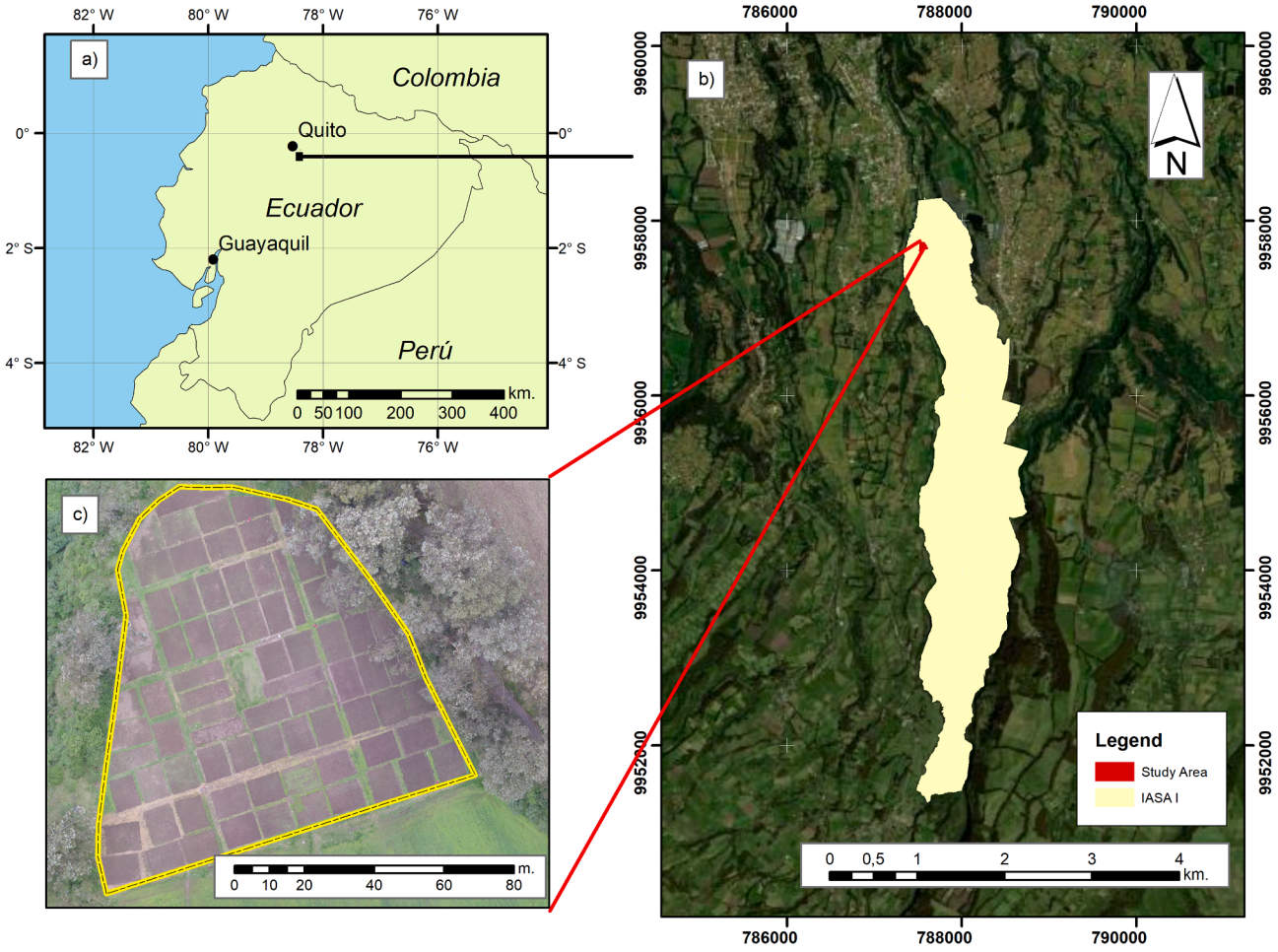

Fig. 1. Location of the study area in (a) Ecuador and more specifically within the (b) IASA I farm; (c) photogrammetry-derived orthomosaic representation of the initial stage of the plots (bare ground). The yellow line represents the limits of the experimental plots. (For interpretation of the references to colour in this figure legend, the reader is referred to the web version of this article.)

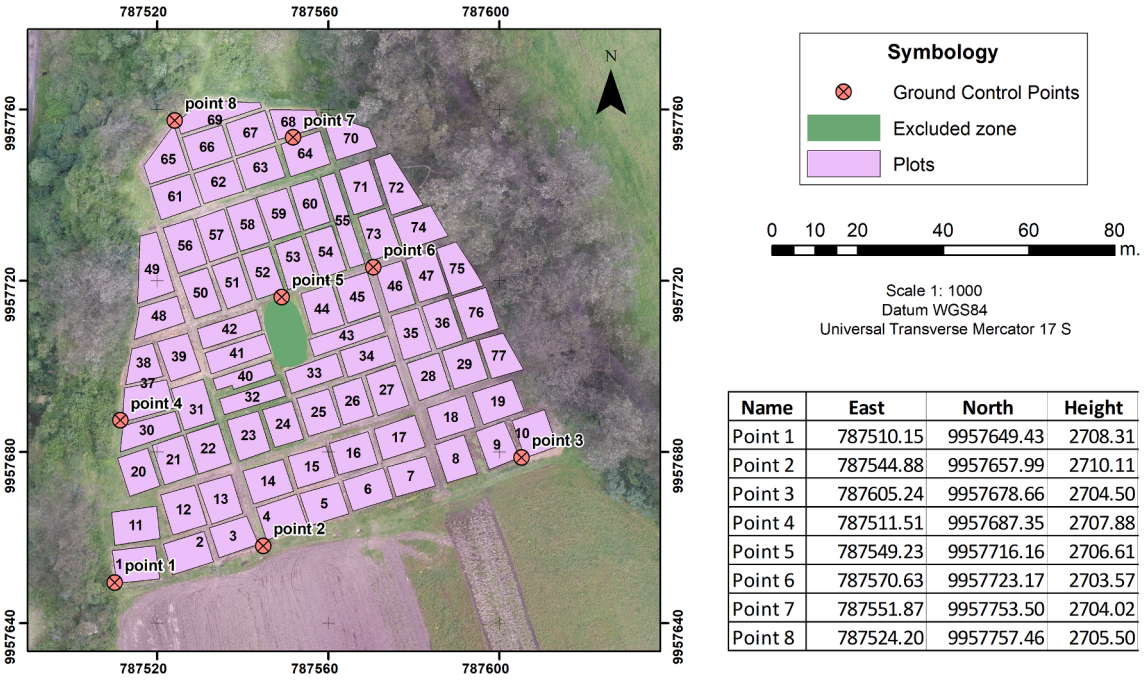

Name	East	North	Height
Point 1	787510.15	9957649.43	2708.31
Point 2	787544.88	9957657.99	2710.11
Point 3	787605.24	9957678.66	2704.50
Point 4	787511.51	9957687.35	2707.88
Point 5	787549.23	9957716.16	2706.61
Point 6	787570.63	9957723.17	2703.57
Point 7	787551.87	9957753.50	2704.02
Point 8	787524.20	9957757.46	2705.50

Fig. 2. Distribution of ground control points.

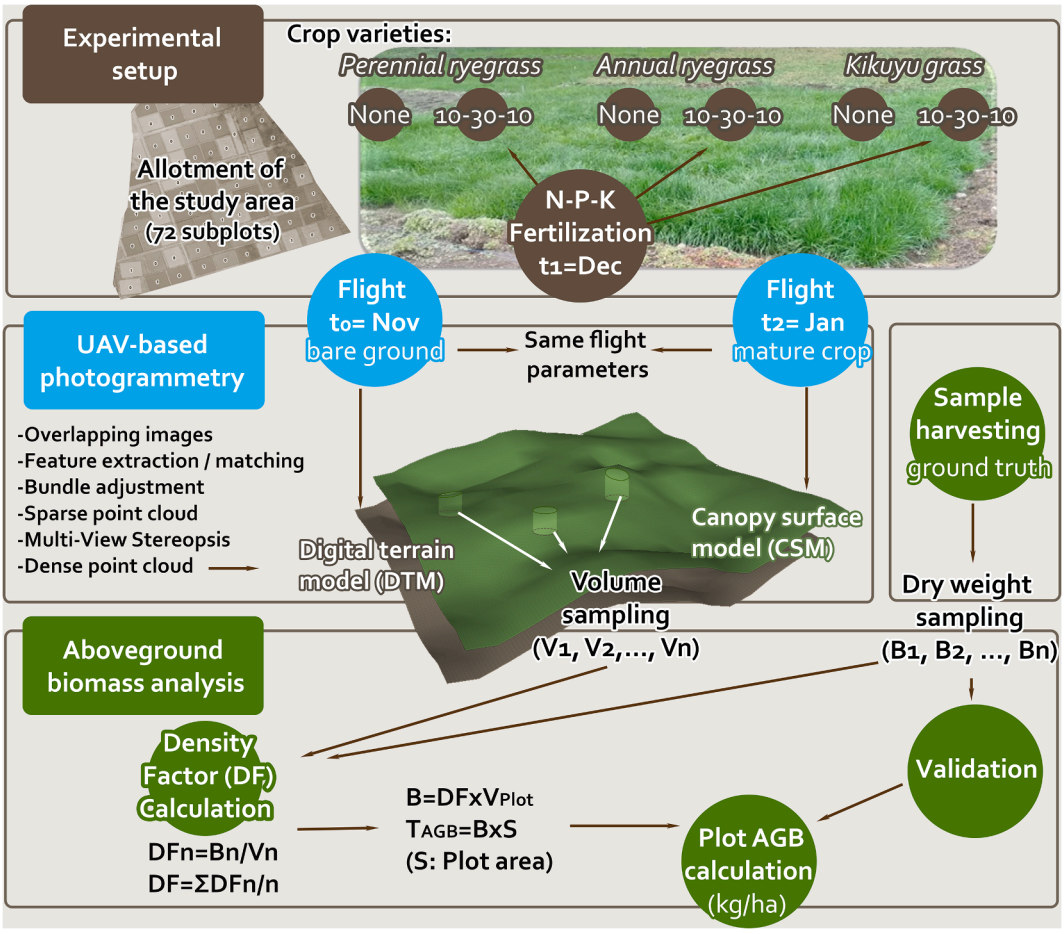

Fig. 3. Methodology implemented in the study.

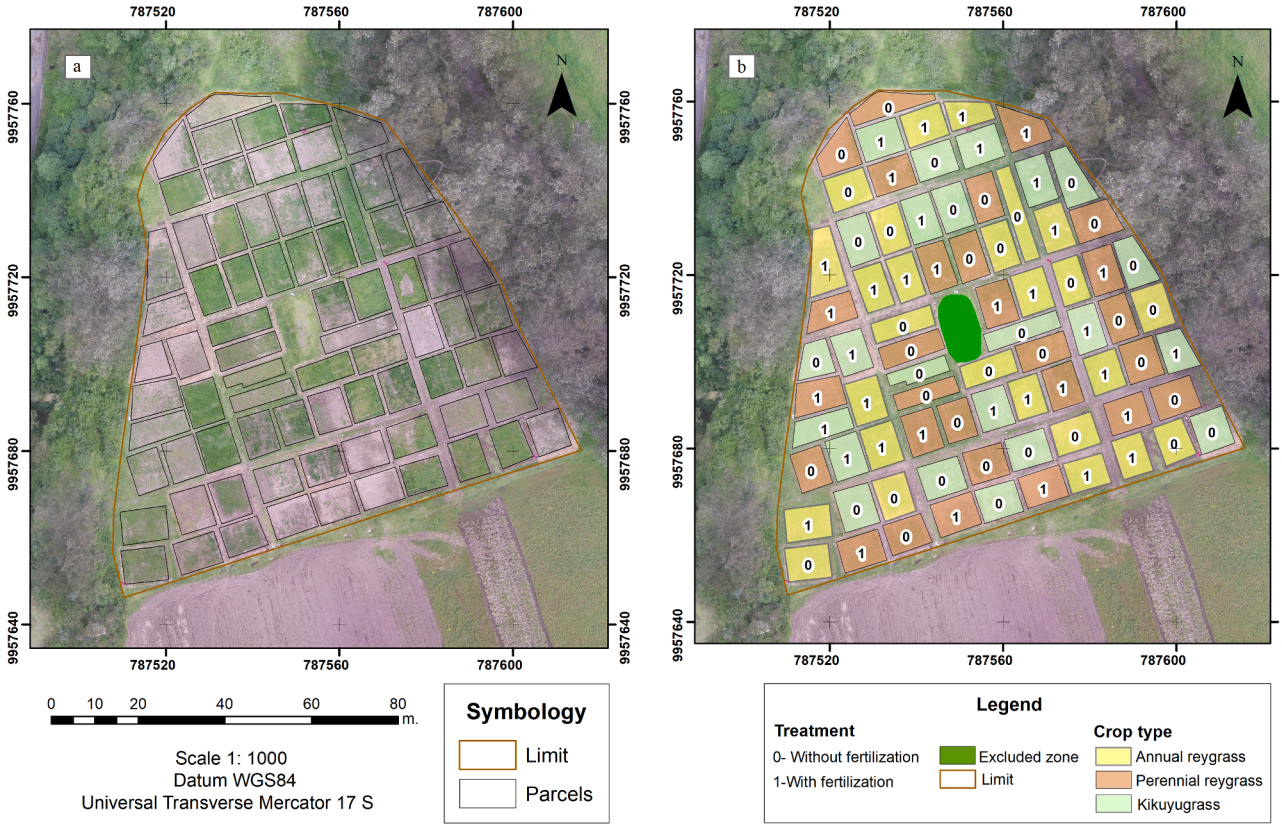

Fig. 4. Experimental setup. Plotting (a) and classification of the pasture crops by crop type and fertilization (b).

of fertilization is ideal for short-cycle crops and aids in plant development and growth (Ñústez, Santos, Navia, & Cotes, 2006).

The three species in this study were perennial ryegrass (*Lolium perenne*), annual ryegrass (*Lolium multiflorum*) and kikuyugrass (*Pennisetum clandestinum*).

2.4. Flight plan and DTM/CSM generation

Flights were performed on November 11th, 2017, which was only one day before planting, and January 16th, 2018, which corresponded to the maximum crop maturity before the first cut. Table 1 shows the flight parameters.

To achieve the required level of detail for a fine-scale grass volume analysis, a maximum GSD of 3 cm for digital models was established. Considering the parameters of the UAV camera, a flight height of 70 m was planned to obtain the desired GSD. To ensure the accuracy and quality of the digital models, high overlaps among the images were implemented. The CSM was derived from a second flight (in January) to determine the crop volume within 54 plots. In addition, based on the November DTM and raster layers extracted from January, the difference in volume between the two surfaces was obtained (Fig. 5).

With the images obtained by the UAV, the SfM software begins by generating the DTM and CSM with an automatic orientation of the photos using a high-accuracy photo alignment procedure; then, a cloud of sparse points is generated, and a high-quality step dense cloud is subsequently produced. This point cloud is a set of points with X, Y, Z coordinates in a reference system. At this moment of the procedure, the point cloud has no real coordinates; however, to continue with the workflow, it is necessary to ingress and mark GCPs. Based on the GCP marking, a spatially referenced dense point cloud was achieved, where the mesh in the built mesh procedure was used to improve the positioning of the markers. The images that corresponded to an initial campaign performed in November, when the terrain was free of vegetation, were used to obtain the reference DTM. The next flight was performed in January, and these images were used to obtain the CSM.

Table 1
Flight parameters.

	First flight (bare ground)	Second flight
Data	November 11th, 2017	January 16th, 2018
Flight height (m)	70	70
Forward overlap	80%	80%
Side overlap	70%	70%
GSD (cm/pixel)	3.06	3.06
Flight time (min)	9	7
No. images	110	86
RMSE X (m)	0.072	0.069
RMSE Y (m)	0.051	0.068
RMSE Z (m)	0.098	0.100

2.5. Crop sampling

The sampling for field biomass estimation was random and destructive; i.e., all organic material was collected within the surface of the sampling area. All samples were harvested immediately after the second flight and on the same day (January 16th, 2018). For each plot, a sample was taken following the methodology of Bendig et al. (2014). A metal ring with an area of 0.25 m^2 was used to define the limits of each sampling, and samples were collected at the coordinates at the centre of the ring. The samples were taken to the laboratory, where they were first weighed wet and subsequently weighed dry after drying for 24 h in an oven. The detailed steps of this procedure are shown in Fig. 5.

These samples were georeferenced based on the total number of plots and a benchmark site inside the study area. One pasture sampling point was taken per plot, so there were 54 random samples in total, 10 of which were used to verify the results. Their distribution is shown in Fig. 6.

Fig. 5. Field culture sampling: a) metal ring, b) cutting, c) sample point georeferencing, d) collection, e) drying and f) measurement of the dry weight of each sample.

2.6. Density factor and aboveground biomass calculation

The DF defined by Gil-Docampo et al. (2020) is a constant derived from the amount of biomass per volume unit that can correct the volume variations (assuming that a larger volume is obtained if the vegetation layer is high and dense, and a lower volume is obtained if the vegetation layer is low and sparse) and produce an objective calculation of biomass in a larger area.

The DF for each sampling point is given by Eq. (1):

$$DF = \frac{B_s}{V_s} \quad (1)$$

where:

DF: density factor [kg·m^{-3}]
B_s: biomass at the sampling point of 0.25 m^2 [kg].
V_s: volume (determined by the difference: CSM-DTM) after crop growth [m^3].

Notably, the value of the DF is not a physical indicator within the plot but a value that enables the corrections of the biomass production with different volumetric values calculated in a CSM of a crop. The DF of the crop was identified at a sample point because it represents the base value for a mass calculation or generalization per experimental unit.

The aboveground biomass was calculated based on the difference in volume per parcel obtained from UAV-derived DTMs and CSMs and the DF of each sample crop. By extracting the raster by parcel from the two models, the volume between the total surfaces of both rasters was calculated. Each plot resulted in a specific volume; thus, the total biomass per plot was determined by equation (2).

$$B_p = DF\hat{A}\cdot V_p \quad (2)$$

where:

B_p: biomass of the plot [kg]
DF: Density Factor [kg·m^{-3}]
V_p: volume (determined by the difference: CSM-DTM) after crop growth [m^3] in each plot.

The DF parameter enables the correction of the correlation between weight and biomass according to the volume extracted with UAV imaging. The wet weight does not always reflect a better crop yield because water accumulated on the grass can dilute the nutritional value per unit weight and increase the cost of nutrients.

2.7. Validation

First, the DTM-CSM coupling was validated by randomly selecting 30 homologous points on bare ground in both models and comparing the results to ensure the adjustment.

Second, the aboveground biomass estimation was validated from 10 reserved field samples. The biomass of the field crop samples to be validated was obtained, the difference between CSM and MDT in the georeferenced sample was determined, and Eq. (2) was applied to the sample to calculate the estimated biomass. A final correlation value and descriptive statistics were obtained between the estimated and measured biomass.

To determine whether the biomass estimation methodology in this study could differentiate between cultivars and treatments, a variance analysis and Fisher's test were performed to differentiate classes among the experimental units.

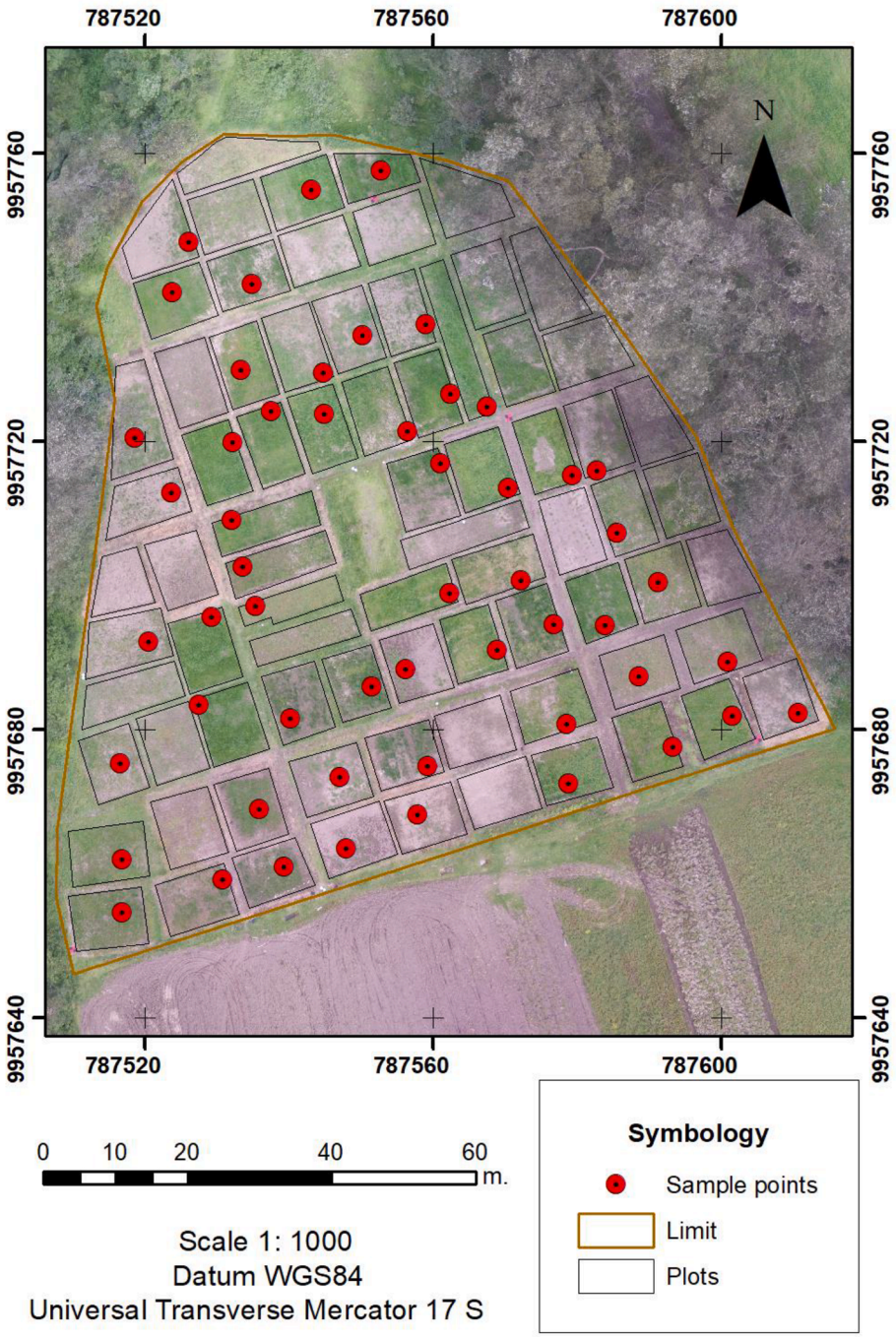

Fig. 6. Biomass sample distribution.

3. Results

3.1. Obtaining the digital models

The initial growth values between models were compared at the raster level. Each pixel in the raster has a different value, which was calculated to obtain the volume between the CSM and the sample DTM.

Finally, at this point, the digital models were compared through the plot-by-plot pixel difference. The difference between DTM and CSM is clearly visible from the rough texture (see Fig. 7).

3.2. Density factor and dry biomass per plot

To estimate the biomass by volume with the UAV images, the sample biomass of each experimental plot was first determined. To differentiate the dry biomass produced by each plot, the DF was considered.

The production of perennial ryegrass, annual ryegrass and kikuyu-grass was 1471 kg/ha, 2121 kg/ha and 1666 kg/ha, respectively, and the corresponding fertilized plots yielded 1483 kg/ha, 2632 kg/ha and 1244 kg/ha. The average parameters for the biomass estimation are shown in Table 2.

3.3. Validation of results

The validation of the DTM-CSM coupling achieved an RMSE Z below 6 cm in all cases (from 30 random samples in bare ground), which confirms the z-positional accuracy of the models.

With the proposed validation of the methodology, an R2 value of

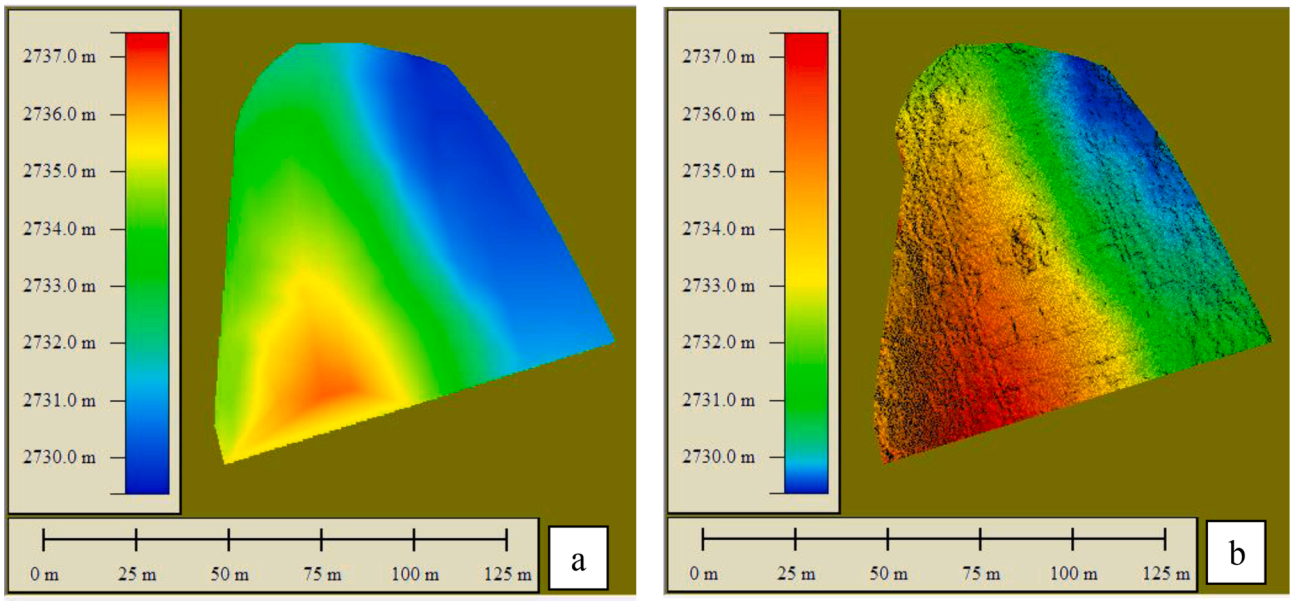

Fig. 7. Multitemporally derived models from UAV-based photogrammetry: a) t_0 = DTM (November) and b) t_2 = CSM (January).

Table 2
Summary of the average analysed factors.

Crop type	Fert.	Number of plots	Av. Volume (m^3)/plot	Av. DF (g/m^3)	Av. Biomass (kg)/plot	Av. Biomass (kg/ha)
PERENNIAL RYEGRASS	YES	11	41.75	328.94	11.30	1483
PERENNIAL RYEGRASS	NO	12	44.09	284.78	11.45	1471
ANNUAL RYEGRASS	YES	13	48.46	488.66	20.41	2632
ANNUAL RYEGRASS	NO	11	45.91	376.13	16.25	2121
KIKUYUGRASS	YES	2	43.71	225.70	9.53	1244
KIKUYUGRASS	NO	5	37.7	315.70	11.58	1666

0.78 was obtained for the calculated biomass between digital processing and field measurement results, which implies a high positive correlation. The validation results are shown in Fig. 8.

To determine whether the biomass estimated via the proposed method can identify significant differences among species or treatments, a variance analysis was implemented (Table 3). Both normality and homoscedasticity premises have been fulfilled; thus, a parametric test such as ANOVA can be used. As shown in Table 3, the p-value was less than 0.05, and significant differences were found between treatments. Once the ANOVA showed that there were significant differences between treatments, LSD Fisher's test was employed to differentiate between classes (treatments).

Fertilization improved the growth of annual ryegrass and perennial ryegrass, which showed increases in biomass per ha production of 19.3% and 0.88%, respectively, compared to the unfertilized plots. Fisher's test analysis found that the biomass of annual ryegrass with fertilization was significantly different from that of the other species and treatments. Thus, this method can characterize annual ryegrass with fertilization but not the other species or treatments. For kikuyugrass, fertilization decreased the production by 25.3%.

4. Discussion

In the present study, a 6-cm accuracy for DTM-CSM coupling was

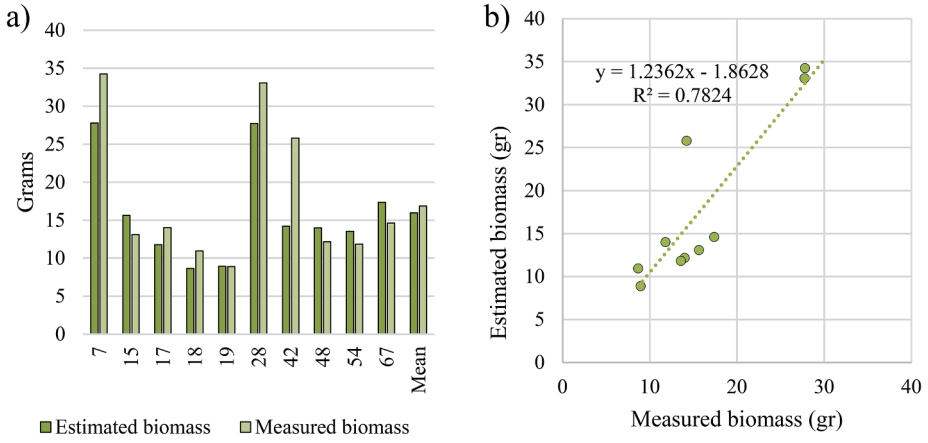

Fig. 8. Comparison of the biomass calculated via digital processing and from field data. a) Bar chart comparison; b) Linear regression.

Table 3
Variance analysis and Fisher's test of the generated biomass per hectare.

VARIABLE	*N*	R^2		$R^2t.$	*C.V.*	
BIOMASS	54	0.44		15,962	31.51	
Variance origin	***Quadratic sum***	***liberty grades***	***Quadratic Average***	***F***	***P-VALUE***	***crit. value***
mODEL	802.22	5	18.20	7.68	<0.0001	0.05
COLUMN	802.22	5	67.81	7.68	<0.0001	0.05
ERROR	1002.39	48	20.88			
Total	1804.61	53				

Variety	*Average*	*n*	*e.e.*	*class*
KikuyuGRASS with fert.	9.53	2	3.23	A
perennial ryegrass without FERT.	11.30	12	1.32	A
perennial ryegrass with fert.	11.45	11	1.38	A
KIKUYUGRASS without FERT.	11.69	5	2.04	A
annual ryegrass without FERT.	16.25	11	1.38	A
annual ryegrass with FERT.	20.42	13	1.27	B

Variance analysis table (SC type III).
Test: LSD Fisher α = 0.05 MSD = 5.41527.
Error: 20.8831.

possible. This level of accuracy is necessary for analysing smaller-size crops such as pasture, and it is much higher than that of the method of Gil-Docampo et al. (2020), who achieved a Z positional accuracy of 23 cm between models of different sources. A DTM of bare ground obtained from a previous UAV flight with the same flight parameters and GCPs has been demonstrated to simplify the process and improve the accuracy of the coupling DTM-CSM; thus, a more precise estimation of the volumes can be expected. Despite this accuracy, the correlation between field samples and estimated values was slightly higher and had an R^2 of 0.88. This finding may be due to the low number of samples used for validation, which was higher in the present study. Meanwhile, poorer results for the correlation could be caused by the size of the crop because a smaller crop can lead to more significant errors. The number of field samples for validation was approximately 20% of the total amount, which was similar to the results of Bendig et al. (2014), who used 30% of the samples in total.

Regarding the correlations, Bendig et al. (2014) obtained R^2 values of 0.92 for summer barley, while Ballesteros et al. (2018) obtained a value of 0.76 for onion, and these studies had GSDs of 0.009 m. and 0.010 m, respectively. Although the GSD in this study was 0.03 m, the correlation was similar.

The DF was used to estimate the biomass, which was similar to the method by Gil-Docampo et al. (2020) for cereal crops. Despite different methodologies, the R2 value between the samples and estimated values of biomass was 0.78, which is similar to those of Batistoti et al. (2019) and Grüner et al. (2019)

An additional analysis in this study was to determine whether fertilization treatments could affect the biomass production in different species of grasslands. Bendig et al. (2014) used different N treatments and modelled the behaviour of the crop to estimate the biomass. In this study, we attempted to identify significant differences among treatments by statistically analysing the estimated biomass in each plot.

According to crop observations, the annual ryegrass had a greater volume and biomass. The 10-30-10 NPK fertilization scheme resulted in significant differences in biomass between kikuyugrass and annual ryegrass and negatively affected the former. Based on the results of the analysis of variance and Fisher's test, the alternative hypothesis can be accepted because significant differences were observed among different treatments and species. In Fisher's test, a significant difference in biomass was found between the annual ryegrass with fertilization and the other crops under various treatments. The type of soil and crop, the occurrence of a rainy season and timing of fertilization can affect the uptake and efficient absorption of fertilizers.

The results show that annual ryegrass reached the correct level of development, and it was even improved in the fertilized plots. The kikuyugrass showed very poor development, where only 7 plots presented growth, among which only 2 were fertilized. Fertilization led to opposite results from the expected effect in kikuyugrass; this finding should be considered and analysed in subsequent studies to make specific recommendations for this species. The reason may be that kikuyugrass was planted through foliage frames and resulted in irregular growth.

It is difficult to establish a comparison of our results related to the perennial ryegrass biomass estimation with a simple RGB camera in Andean zones, but there are several studies in oceanic climates, such as Borra-Serrano et al. (2019) in Belgium, who found an R^2 of 0.67 for the best-performing height metric in perennial ryegrass, and Lussem et al. (2020) in Germany, who found a variable R^2 of 0.65 between predicted and observed dry biomass yields. In both cases, their results had lower correlation between observed and predicted biomass than the observations in this study which demonstrates that the methodology of the present study can overcome other more common ones.

5. Conclusions

The use of photogrammetry with UAVs enables the estimation of the total biomass, and the yield of the total plot can be generalized (with a few samples in the field) by quantifying the volume. However, the experiments in this work were performed in plots with different treatments, so many samples had to be collected to individually evaluate each treatment.

The biomass of different grass crops was obtained through UAV sensors, which provide substantial economic savings compared to the traditional methods.

The proposed methodology was validated with 10 field-collected samples, and the resulting correlation coefficient (R2) was 0.78 between estimated and observed biomasses, which implies a strong positive correlation between estimated biomass and UAV imaging-obtained biomass in different plots cultivated with the three species (perennial ryegrass, annual ryegrass and kikuyu).

In a significant number of studies, LiDAR methods have been validated for the biomass estimation in different crops, and more studies that implement LiDAR systems with UAVs are recommended to increase the accuracy without sacrificing the yield.

Moreover, optimized field samplings in plots with uniform characteristics and extensions are recommended for further studies. Future studies should focus on the combined analysis of nonspectral and spectral data to take advantage of the benefits of each technique.

CRediT authorship contribution statement

Izar Sinde-González: Conceptualization, Methodology, Investigation, Visualization, Formal analysis, Writing - original draft, Writing - review & editing. **Mariluz Gil-Docampo:** Conceptualization, Investigation, Writing - review & editing. **Marcos Arza-García:** Visualization, Writing - review & editing. **José Grefa-Sánchez:** Validation, Investigation, Methodology, Methodology, Writing - original draft. **Diana Yánez-Simba:** Validation, Investigation, Methodology, Methodology, Writing - original draft. **Patricio Pérez-Guerrero:** Resources, Supervision. **Víctor Abril-Porras:** Resources, Supervision.

Declaration of Competing Interest

The authors declare that they have no known competing financial interests or personal relationships that could have appeared to influence the work reported in this paper.

Appendix A. Supplementary data

Supplementary data to this article can be found online at https://doi.org/10.1016/j.jag.2021.102355.

References

Acevo-Herrera, R., Aguasca, A., Bosch-Lluis, X., Camps, A., Martinez-Fernandez, J., Sanchez-Martin, N., Perez-Gutierrez, C., 2010. Design and first results of an UAV-borne L-band radiometer for multiple monitoring purposes. Remote Sensing 2 (7), 1662–1679. https://doi.org/10.3390/rs2071662.

Acorsi, M.G., das Dores Abati Miranda, Fabiani, Martello, M., Smaniotto, D.A., Sartor, L. R., 2019. Estimating biomass of black oat using UAV-based RGB imaging. Agronomy, 9(7), 344.

Arza-García, M., Gil-Docampo, M., Ortiz-Sanz, J., 2019. A hybrid photogrammetry approach for archaeological sites: block alignment issues in a case study (the roman camp of A cidadela). J. Cult. Heritage 38, 195–203. https://doi.org/10.1016/j.culher.2019.01.001.

Astapov, A.Y., Prishutov, K.A., Krivolapov, I.P., Astapov, S.Y., Korotkov, A.A., 2019. Unmanned aerial vehicles for estimation of vegetation quality. Amazonia Investiga 8 (23), 27–36.

Ballesteros, R., Ortega, J.F., Hernandez, D., Moreno, M.A., 2018. Onion biomass monitoring using UAV-based RGB imaging. Precis. Agric. 19 (5), 840–857.

Bareth, G., Schellberg, J., 2018. Replacing manual rising plate meter measurements with low-cost UAV-derived sward height data in grasslands for spatial monitoring. PFG–J. Photogrammetry, Remote Sensing Geoinformation Sci. 86 (3–4), 157–168.

Batistoti, J., Marcato Junior, J., Ítavo, L., Matsubara, E., Gomes, E., Oliveira, B., Souza, M., Siqueira, H., Salgado Filho, G., Akiyama, T., Goncalves, W., Liesenberg, V., Li, J., Dias, A., 2019. Estimating pasture biomass and canopy height in brazilian savanna using UAV photogrammetry. Remote Sensing 11 (20), 2447.

Belton, D., Helmholz, P., Long, J., Zerihun, A., 2019. Crop height monitoring using a consumer-grade camera and UAV technology. Pfg-J. Photogrammetry Remote Sensing Geoinformation Sci. 87 (5–6), 249–262. https://doi.org/10.1007/s41064-019-00087-8.

Bendig, J., Bolten, A., Bennertz, S., Broscheit, J., Eichfuss, S., Bareth, G., 2014. Estimating biomass of barley using crop surface models (CSMs) derived from UAV-based RGB imaging. Remote Sensing 6 (11), 10395–10412.

Borra-Serrano, I., De Swaef, T., Muylle, H., Nuyttens, D., Vangeyte, J., Mertens, K., Lootens, P., 2019. Canopy height measurements and non-destructive biomass estimation of Lolium perenne swards using UAV imagery. Grass Forage Sci. 74 (3), 356–369.

Busemeyer, L., Mentrup, D., Müller, K., Wunder, E., Alheit, K., Hahn, V., et al., 2013. BreedVision, A multi-sensor platform for non-destructive field-based phenotyping in plant breeding. Sensors, 13(3), 2830-2847.

Calou, V.B.C., Teixeira, A.d.S., Moreira, L.C.J., da Rocha Neto, Odilio C., da Silva, J.A., 2019. Estimation of maize biomass using unmanned aerial vehicles. Engenharia Agricola, 39(6), 744-752. doi:10.1590/1809-4430-Eng.Agric.v39n6p744-752/2019.

Castro, W., Marcato Junior, J., Polidoro, C., Osco, L.P., Gonçalves, W., Rodrigues, L., Matsubara, E., 2020. Deep learning applied to phenotyping of biomass in forages with UAV-based RGB imagery. Sensors 20 (17), 4802.

Catchpole and Wheeler, 2010. Estimating plant biomass: a review of techniques. Austral Ecol. 17 (2010), 121–131.

Cevallos, L.N.M., García, J.L.R., Suárez, B.I.A., González, C.A.L., González, I.S., Campoverde, J.A.Y., et al., 2018. A NDVI analysis contrasting different spectrum data methodologies applied in pasture crops previous Grazing A case study from Wcuador. Paper presented at the 2018 International Conference on eDemocracy & eGovernment (ICEDEG), 126-135.

Cooper, S.D., Roy, D.P., Schaaf, C.B., Paynter, I., 2017. Examination of the potential of terrestrial laser scanning and structure-from-motion photogrammetry for rapid nondestructive field measurement of grass biomass. Remote Sensing 9 (6), 531.

Cucho-Padin, G., Loayza, H., Palacios, S., Balcazar, M., Carbajal, M., Quiroz, R., 2019. Development of low-cost remote sensing tools and methods for supporting smallholder agriculture. Appl. Geomatics 1–17.

Dash, J.P., Watt, M.S., Pearse, G.D., Heaphy, M., Dungey, H.S., 2017. Assessing very high-resolution UAV imagery for monitoring forest health during a simulated disease outbreak. ISPRS J. Photogramm. Remote Sens. 131, 1–14.

d'Oleire-Oltmanns, S., Marzolff, I., Peter, K., Ries, J., 2012. Unmanned aerial vehicle (UAV) for monitoring soil erosion in morocco. Remote Sensing 4 (11), 3390–3416.

Eitel, J.U., Magney, T.S., Vierling, L.A., Brown, T.T., Huggins, D.R., 2014. LiDAR based biomass and crop nitrogen estimates for rapid, non-destructive assessment of wheat nitrogen status. Field Crops Research 159, 21–32.

Fonstad, M.A., Dietrich, J.T., Courville, B.C., Jensen, J.L., Carbonneau, P.E., 2013. Topographic structure from motion: A new development in photogrammetric measurement. Earth Surf. Proc. Land. 38 (4), 421–430.

Frankl, A., Seghers, V., Stal, C., De Maeyer, P., Petrie, G., Nyssen, J., 2015. Using image-based modelling (SfM–MVS) to produce a 1935 ortho-mosaic of the ethiopian highlands. Int. J. Digital Earth 8 (5), 421–430. https://doi.org/10.1080/17538947.2014.942715.

Furukawa, Y., Ponce, J. Accurate, Dense, Robust Multi-View Stereopsis, 2007. In: Proceedings of the IEEE Conference on Computer Vision and Pattern Recognition, Minneapolis, MN, USA, 18–23 June 2007, 1, pp. 1–8.

Gil-Docampo, M.L., Arza-García, M., Ortiz-Sanz, J., Martínez-Rodríguez, S., Marcos-Robles, J.L., Sánchez-Sastre, L.F., 2020. Above-ground biomass estimation of arable crops using UAV-based SfM photogrammetry. Geocarto International 35 (7), 687–699.

Grijalva, J., Espinosa, F., & Hidalgo, M., 1995. Producción y utilización de pastizales en la región interandina del ecuador INIAP Archivo Histórico.

Grüner, E., Astor, T., Wachendorf, M., 2019. Biomass prediction of heterogeneous temperate grasslands using an SfM approach based on UAV imaging. Agronomy 9 (2), 54.

Grüner, E., Wachendorf, M., Astor, T., 2020. The potential of UAV-borne spectral and textural information for predicting aboveground biomass and N fixation in legume-grass mixtures. PLoS ONE 15 (6), e0234703.

Gul, Y., 2019. Applications of unmanned aerial vehicle (UAV) in open-pit mines. Turkiye Jeoloji Bulteni-Geol. Bull. Turkey 62 (1), 99–112. https://doi.org/10.25288/tjb.519506.

Guo, T., Kujirai, T., Watanabe, T., 2012. Mapping crop status from an unmanned aerial vehicle for precision agriculture applications. Xxii Isprs Congress, Technical Commission I 39–B1, 485–490.

Hart, L., Huguenin-Elie, O., Latsch, R., Simmler, M., Dubois, S., Umstatter, C., 2020. Comparison of spectral reflectance-based smart farming tools and a conventional approach to determine herbage mass and grass quality on farm. Remote Sensing 12 (19), 3256.

Iglhaut, J., Cabo, C., Puliti, S., Piermattei, L., O'Connor, J., Rosette, J., 2019. Structure from motion photogrammetry in forestry: a review. Curr. Forestry Rep. 5 (3), 155–168.

Jenal, A., Lussem, U., Bolten, A., Gnyp, M.L., Schellberg, J., Jasper, J., Bareth, G., 2020. Investigating the potential of a newly developed UAV-based VNIR/SWIR imaging system for forage mass monitoring. PFG–J. Photogrammetry, Remote Sensing Geoinform. Sci. 88 (6), 493–507.

Kachamba, D.J., Orka, H.O., Gobakken, T., Eid, T., Mwase, W., 2016. Biomass estimation using 3D data from unmanned aerial vehicle imagery in a tropical woodland. Remote Sensing 8 (11), 968. https://doi.org/10.3390/rs8110968.

Lowe, D.G., 2004. Distinctive image features from scale-invariant keypoints. Int. J. Comput. Vis 60, 91–110.

Lussem, U., Schellberg, J., Bareth, G., 2020. Monitoring forage mass with low-cost UAV data: case study at the Rengen grassland experiment. PFG–J. Photogrammetry, Remote Sensing Geoinform. Sci. 88 (5), 407–422.

Maresma, A., Ariza, M., Martinez, E., Lloveras, J., Martinez-Casasnovas, J.A., 2016. Analysis of vegetation indices to determine nitrogen application and yield prediction in maize (*zea mays L.*) from a standard UAV service. Remote Sensing 8 (12), 973. https://doi.org/10.3390/rs8120973.

Meneses, V.A.B., Téllez, J.M., Velasquez, D.F.A., 2015. Uso de drones para el análisis de imágenes multiespectrales en agricultura de precisión. *@ Limentech, Ciencia Y Tecnología*. Alimentaria 13 (1).

Micheletti, N., Chandler, J.H., Lane, S.N., 2015. Investigating the geomorphological potential of freely available and accessible structure-from-motion photogrammetry using a smartphone. Earth Surf. Proc. Land. 40 (4), 473–486. https://doi.org/10.1002/esp.3648.

Michez, A., Lejeune, P., Bauwens, S., Herinaina, A.A.L., Blaise, Y., Castro Muñoz, E., Bindelle, J., 2019. Mapping and monitoring of biomass and grazing in pasture with an unmanned aerial system. Remote Sensing 11 (5), 473.

Michez, A., Philippe, L., David, K., Sébastien, D., Christian, D., Bindelle, J., 2020. Can low-cost unmanned aerial systems describe the forage quality heterogeneity? Insight from a Timothy Pasture Case Study in Southern Belgium. Remote Sensing 12 (10), 1650.

Mukherjee, A., Misra, S., Raghuwanshi, N.S., 2019. A survey of unmanned aerial sensing solutions in precision agriculture. J. Network Computer Appl. 148, 102461. https://doi.org/10.1016/j.jnca.2019.102461.

Näsi, R., Viljanen, N., Kaivosoja, J., Alhonoja, K., Hakala, T., Markelin, L., Honkavaara, E., 2018. Estimating biomass and nitrogen amount of barley and grass using UAV and aircraft based spectral and photogrammetric 3D features. Remote Sensing 10 (7), 1082.

Nawaz, H., Ali, H.M., Massan, S., 2019. *Applications of unmanned* aerial vehicles: a review. 3c Tecnologia SI, 85–105. https://doi.org/10.17993/3ctecno.2019.specialissue3.85-105.

Niu, Y., Zhang, L., Zhang, H., Han, W., Peng, X., 2019. Estimating above-ground biomass of maize using features derived from UAV-based RGB imagery. Remote Sensing 11 (11), 1261.

Ñústez, C.E., Santos, M., Navia, S.L., Cotes, J.M., 2006. Evaluación de la fertilización fosfórica foliar y edáfica sobre el rendimiento de la variedad de papa'diacol capiro'(*solanum tuberosum L.*). Agronomía Colombiana 24 (1), 111–121.

Pepe, M. Constantino, D., 2020. UAV Photogrammetry and 3D Modelling of Complex Architecture for Maintenance Purposes: the Case Study of the Masonry Bridge on the Sele River, Italy. Periodica Polytechnica Civil Engineering, 65(1), pp. 191-203, 2021.

Pepe, M., Constantino, D., Alfio, V.S., Zannotti, N., 2020. 4D Geomatics monitoring of a quarry for the calculation of extracted volumes by TIN and Grid model: contribute of UAV photogrammetry. *Geographia Technica,* 16. Special Issue 2021, 1–14.

Selsam, P., Schaeper, W., Brinkmann, K., Buerkert, A., 2017. Acquisition and automated rectification of high-resolution RGB and near-IR aerial photographs to estimate plant biomass and surface topography in arid agro-ecosystems. Exp. Agric. 53 (1), 144–157.

Stroppiana, D., Migliazzi, M., Chiarabini, V., Crema, A., Musanti, M., Franchino, C., Villa, P., 2015. Rice yield estimation using multispectral data from uav: a preliminary experiment in northern italy. Ieee Int. Geosci. Remote Sensing Symposium (Igarss) 2015, 4664–4667.

Tilly, N., Hoffmeister, D., Cao, Q., Huang, S., Lenz-Wiedemann, V., Miao, Y., Bareth, G., 2014. Multitemporal crop surface models: accurate plant height measurement and biomass estimation with terrestrial laser scanning in paddy rice. J. Appl. Remote Sens. 8 (1), 083671.

Torres-Sánchez, J., López-Granados, F., Serrano, N., Arquero, O., Peña, J.M., 2015. High-throughput 3-D monitoring of agricultural-tree plantations with unmanned aerial vehicle (UAV) technology. PLoS ONE 10 (6), e0130479.

Viljanen, N., Honkavaara, E., Näsi, R., Hakala, T., Niemeläinen, O., Kaivosoja, J., 2018. A novel machine learning method for estimating biomass of grass swards using a photogrammetric canopy height model, images and vegetation indices captured by a drone. Agriculture 8 (5), 70.

Waite, 1994. The application of visual estimation procedures for monitoring pasture yield and composition in exclosures and small plots. Tropic. Grasslands, 20 (1994), pp. 1-27.

Westoby, M.J., Brasington, J., Glasser, N.F., Hambrey, M.J., Reynolds, J.M., 2012. 'Structure-from-Motion'photogrammetry: a low-cost, effective tool for geoscience applications. Geomorphology 179, 300–314.

Zhu, W., Sun, Z., Peng, J., Huang, Y., Li, J., Zhang, J., Liao, X., 2019. Estimating maize above-ground biomass using 3D point clouds of multi-source unmanned aerial vehicle data at multi-spatial scales. Remote Sensing 11 (22), 2678. https://doi.org/10.3390/rs11222678.